



Minerva Access is the Institutional Repository of The University of Melbourne

Author/s:

Reid, KJ;O'Brien, TA;King, AD;Lane, TP

Title:

Extreme Water Vapor Transport During the March 2021 Sydney Floods in the Context of Climate Projections

Date:

2021-11-28

Citation:

Reid, K. J., O'Brien, T. A., King, A. D. & Lane, T. P. (2021). Extreme Water Vapor Transport During the March 2021 Sydney Floods in the Context of Climate Projections. *Geophysical Research Letters*, 48 (22), <https://doi.org/10.1029/2021GL095335>.

Persistent Link:

<https://hdl.handle.net/11343/299216>

Extreme Water Vapor Transport during the March 2021 Sydney Floods in the Context of Climate Projections

Kimberley J. Reid¹, Travis A. O'Brien^{2,3}, Andrew D. King¹ and Todd P. Lane¹

¹*Australian Research Council Centre of Excellence for Climate Extremes and School of Geography, Earth and Atmospheric Sciences, The University of Melbourne, Parkville, Australia*

²*Earth and Atmospheric Sciences Department, Indiana University, Bloomington, IN, USA*

³*Climate and Ecosystem Sciences Division, Lawrence Berkeley National Lab, Berkeley, CA, USA*

Abstract

During March 2021, large regions of Eastern Australia experienced prolonged heavy rainfall and extensive flooding. The maximum daily mean column integrated water vapor transport (IVT) over Sydney during this event was within the top 0.3% of all days since 1980, and the 10-day mean IVT was in the top 0.2%. In this study, we have examined the change in frequency of extreme IVT events over Sydney in sixteen climate models from the Coupled Model Intercomparison Project 6 under two Shared Socioeconomic Pathways (SSP245 and SSP585). Generalized Extreme Value modelling was used to further analyze the change in frequency of extreme IVT events. We found the probability of long duration high IVT events is projected to increase by 80% at the end of the century, but the future change in IVT is correlated to the rate of global and regional warming in each model.

Plain Language Summary

This is the author manuscript accepted for publication and has undergone full peer review but has not been through the copyediting, typesetting, pagination and proofreading process, which may lead to differences between this version and the [Version of Record](#). Please cite this article as [doi: 10.1029/2021GL095335](https://doi.org/10.1029/2021GL095335).

This article is protected by copyright. All rights reserved.

During March 2021, large regions of Eastern Australia experienced prolonged heavy rainfall and extensive flooding. This was associated with strong horizontal water vapor transport over this region that persisted for approximately 10 days. The amount of water vapor transported over Sydney during this event was extreme and within the top 0.3% of all days since 1980. In this study, we used climate models to project how much more often events such as these may occur by the end of the 21st Century under two greenhouse gas emission scenarios. We found that the probability of long duration high water vapor transport over Sydney, as in March 2021, may increase by 80%.

Key Points

Sydney's March 2021 floods were associated with persistent high water vapor transport.

The probability of long-duration high IVT events should increase by the end of the 21st Century.

Differences in climate sensitivity within the CMIP6 ensemble may increase the spread of moisture flux projections.

Introduction

Between the 17th and 24th of March 2021, much of eastern Australia experienced heavy rainfall and wide-spread flooding. During that period, the entire coastline of New South Wales (NSW) received more than 200mm of rain and in some locations more than 400mm of rain fell (The Bureau of Meteorology, 2021). Sydney (Observatory Hill Automatic Weather Station) recorded 212.4mm of rain between the 19th-21st of March 2021 with 110.4mm falling on the 21st.

The March 2021 event was associated with a blocking anticyclone in the Tasman Sea; the easterly flow advected moist air over the east coast (Fig 1a) followed by the convergence of

moisture from two regions (Fig1b-c). Most of the rainfall records occurred on the 23rd of March when the intense Atmospheric River moved over the east coast. This event received much media attention and public commentary about the potential role of climate change in this event. However, weather events like this are not necessarily uncommon. For example, in January 2012, a blocking high in the Tasman followed by strong southward moisture flux led to wide-spread flooding over eastern NSW (The Bureau of Meteorology, 2012). For both events the strength and duration of the moisture flux is likely of critical importance. The purpose of this paper is to place this recent event in the context of the prior observational record and future climate projections by examining the water vapor transport.

Atmospheric rivers (ARs) are associated with localized regions of high integrated vapor transport (IVT), which is defined as the column-averaged horizontal transport of water vapor mass. A northwesterly AR impacted Sydney between the 21st-23rd of March. However, there was high IVT over Sydney in the days prior which does not continuously satisfy the criteria for an AR. For this reason, we focus on IVT throughout this study.

It has been established that IVT is a strong predictor for precipitation (Lavers & Villarini, 2015) and Rutz et al., (2014) showed that the spatial extent of IVT correlated more strongly with precipitation than total column water vapour over land. Lavers et al., (2014) found that large scale horizontal moisture transport is more predictable than precipitation and could be used to extend the forecast lead time of extreme precipitation by up to 3 days in some locations over Europe. There is a large body of literature documenting the association of IVT, extreme rainfall, flooding and ARs worldwide (e.g. Corringham et al., 2019; Gimeno et al., 2016; Reid et al., 2021; Viale et al., 2018).

Understanding extreme rainfall and flooding events around Sydney is important due to its large population and economic value (Nicholls, 2006), but precipitation, and especially extreme precipitation, is poorly simulated in global climate models (Stephens et al., 2010).

Given the strong relationship between IVT and precipitation, the prominent role of IVT during the March 2021 (and previous) East Australian flooding, and the higher predictability of IVT compared to extreme precipitation (Lavers et al., 2014), understanding changes to IVT in a warmer world is necessary for preparing for future hydrological extremes in this region. Hence, the aim of this paper is to understand IVT over Sydney in the context of climate projections.

Warner et al., (2015) analysed IVT projections along the West Coast of the USA in the Coupled Model Intercomparison Project (CMIP) 5 models under Representative Concentration Pathway (RCP) 8.5 and found significant increases in water vapor transport as anthropogenic greenhouse gas concentrations rise. Studies of Southern Hemisphere ARs have suggested a poleward shift in ARs in recent decades, and hence regions of enhanced IVT, due to changes in the location of the westerly jet (Ma et al., 2020; Swart et al., 2015). However, projections of IVT over Australia have not been adequately assessed.

In this paper, we evaluated the CMIP6 multi-model ensemble of IVT over Sydney (Australia's most populated city) and used the best performing models to project the end-of-century IVT response to 'middle-of-the-road' and 'business-as-usual' climate change scenarios using simulations from the ScenarioMIP (Eyring et al., 2016). We also use Generalized Extreme Value (GEV) modelling to estimate the change in likelihood of extreme IVT events that are a similar duration and intensity to the March 2021 event under global

warming. Finally, we assessed the role that the rate of global and regional warming in models may contribute to uncertainty in IVT projections.

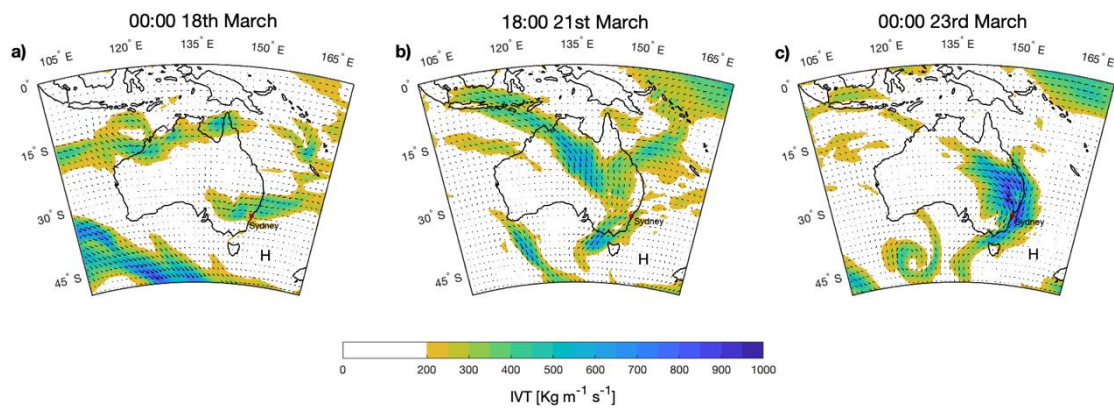


Figure 1: Integrated Water Vapour Transport from ERA5 at a) 0000z 18th March, b) 1800z 21st March and c) 0000z 23rd March 2021. Colors show the magnitude and vectors show the direction of IVT. The H symbol indicates the quasi-stationary high pressure.

Methods

We used daily IVT (determined from hourly data) between 1980-2014 (end of the historical model runs) from ERA5 Copernicus Climate Change Service (Hersbach et al., 2019) along a transect of the East Australian Coast (28°S to 38°S) to evaluate the climatology of IVT in this region and determine how unusual the March 2021 event was. We also used daily atmospheric surface temperature, specific humidity, and horizontal winds from sixteen CMIP6 models (Supplementary Table 1) and evaluated IVT by calculating the mass-weighted integral of the product of specific humidity and horizontal winds between 300hPa and 1000hPa (or the surface where topography exceeded the 1000hPa level). Only the first

ensemble member was used, as in Warner et al., (2015), to avoid biasing towards models with more ensemble members. We used the historical (1980-2014) run for model evaluation and our climate baseline, and the Shared Socioeconomic Pathways (SSP) SSP245 and SSP585 future scenarios (2080-2100; O'Neill et al., 2016). We chose to focus on the period between 2080 and 2100 to maximise the warming signal and better understand the climate change influence on IVT.

All models and the ERA5 reanalysis were regridded to a $2^\circ \times 2^\circ$ horizontal resolution using bilinear interpolation. We used an initial domain of 150°E - 154°E longitude, and 28°S to 38°S latitude. The IVT was averaged across the longitude dimension to produce a transect of IVT approximately parallel to the East Coast of Australia. We then focussed on the grid centered on 34°S , which includes Sydney. Sixteen CMIP6 models were chosen based on data availability. We used quantile-quantile analysis and calculated the root mean squared error (RMSE) of the historical model runs versus ERA5 quantiles (Supplementary Table 1) and the reference line (ERA5 versus ERA5) similar to Perkins et al., (2007). We calculated the RMSE for all quantiles and for just the upper quartile. We then selected the best eight models based on which models produced the lowest RMSE over the whole distribution and the upper quartile, which happened to be the same models. Model evaluation is discussed further in the results section.

We calculated the March-April-May (MAM) maximum of the 10-day average IVT (IVT \times 10day) for each model as that was the approximate duration for the March 2021 event. We fit a non-stationary GEV to the IVT \times 10day combined data from the historical and SSP245 simulations and historical and SSP585 simulations, modelling the location parameter (μ) as varying linearly in time (t) as in Risser and Wehner, (2017): $\mu(t) = c_\mu t + \mu_0$. The

posterior distribution was sampled using a Bayesian approach and the Emcee package (Foreman-Mackey et al., 2019). The quasi-uniform prior restricts the posterior distribution to Type I (Gumbel) and Type II (Fréchet) distributions, based on the prior assumptions that the distribution of IVTx10day should be positively skewed. Ten Markov Chain Monte Carlo (MCMC) chains for 11,000 steps were run retaining only the final 100 samples. This calculation was repeated on each of the CMIP6 models. This results in 1,000 estimates i of the GEV model parameters $c_{\mu}^{i,m}$, $\mu_0^{i,m}$ (*location or mean*), $\sigma^{i,m}$ (*scale or variance*), $\xi^{i,m}$ (*shape or skewness*) for each CMIP6 model m .

We do a similar GEV fit to ERA5 data and calculate the percentile of the March 2021 event; we use the mode of the percentiles as the 2021 reference value from which to calculate probability ratios. We then determine the percentile value of IVT, X_t , in the year 2021 from the model-based MCMC samples. We refer to these IVT values as $IVT_0^{i,m}$. We calculate the Probability Ratio (PR) of such an IVTx10day value occurring in the years 2080-2100 as:

$$\begin{aligned}
 PR^{i,m} &= \frac{P(IVT > IVT_0^{i,m} | t = 2021, c_{\mu}^{i,m}, \mu_0^{i,m}, \sigma^{i,m}, \xi^{i,m})}{P(IVT > IVT_0^{i,m} | t = 2100, c_{\mu}^{i,m}, \mu_0^{i,m}, \sigma^{i,m}, \xi^{i,m})} \\
 &= \frac{1 - X_t/100}{P(IVT > IVT_0^{i,m} | t \in (2080,2100), c_{\mu}^{i,m}, \mu_0^{i,m}, \sigma^{i,m}, \xi^{i,m})}
 \end{aligned}
 \tag{1}$$

Climatology and Context

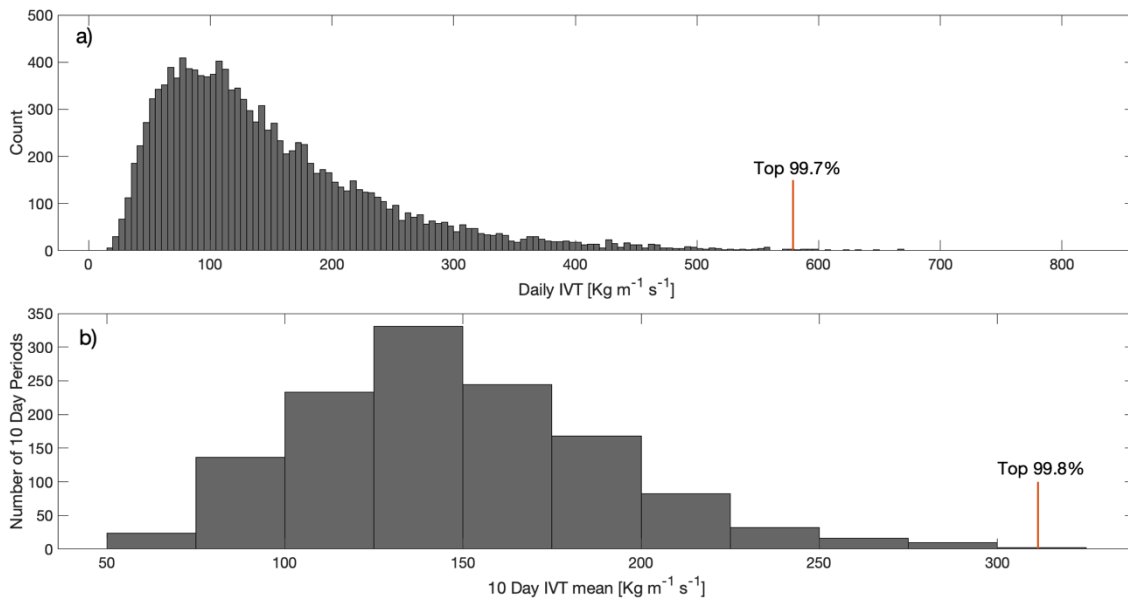


Figure 2: Histograms of a) daily mean IVT over Sydney and b) 10-day mean IVT between 1980-2014 from ERA5. The red lines indicate the peak daily (a) and 10-day mean (b) IVT during the March 2021 flooding event and the values above the red lines are the percentiles of that IVT value relative to the climatology.

Figure 2 shows the distribution of IVT values over Sydney between 1980-2014 for all seasons. Extreme IVT events are not limited to MAM so we include all seasons for the analysis in Figures 2 and 3. The climatology of IVT indicates that water vapor flux during this flooding event was unusual in both peak intensity and persistence (indicated by the 10-day mean IVT). Over the Sydney region, the maximum daily mean IVT was in the top 0.3% and the 10-day mean IVT was the 3rd highest since 1980 (Figure 2b). The two 10-day mean IVT events that exceeded the March 2021 event were also associated with widespread heavy rainfall and flooding. Similar, to the 2021 event, both events were associated with a large-

scale cloudband extending from the northwest (satellite imagery; not shown). The rank of the March 2021 IVT in the climatology indicates that this was indeed an extreme IVT event as well as an extreme rainfall and flooding event. The next section of this paper looks at how IVT over these locations may change with anthropogenic climate change. We note that we do not observe a trend in IVT over the historical period in ERA5 (1980-2014) for this domain and there is strong interannual variability in annual mean and maximum IVT over Sydney.

Future Projections of IVT

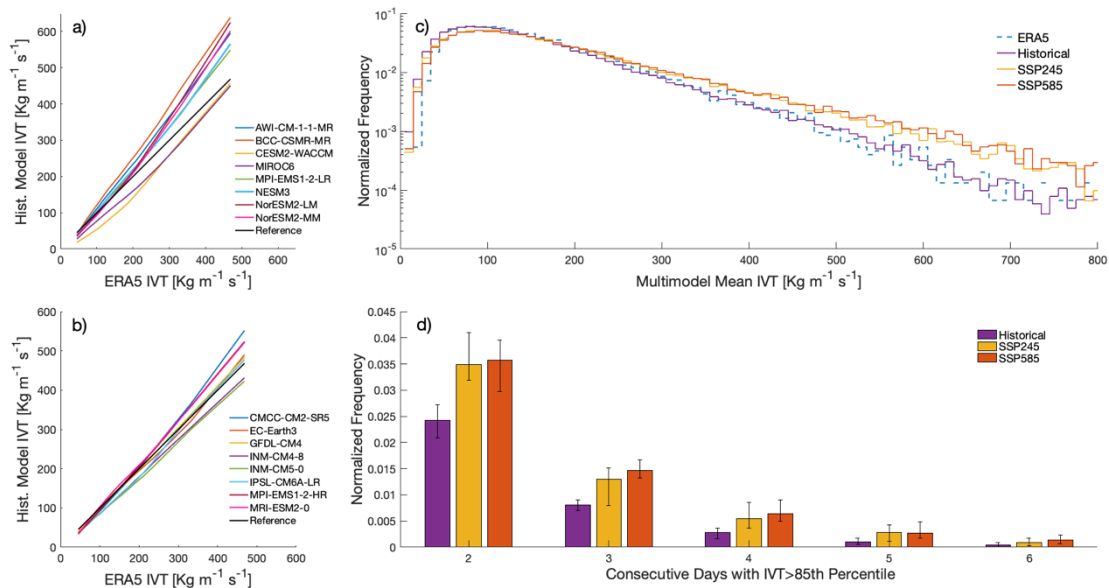


Figure 3: Quantile-quantile plot of ERA5 IVT and historical model IVT [$\text{Kg m}^{-1} \text{s}^{-1}$] for the worst 8 (a) and best 8 (b) models at 34S. The black line represents the ERA5 IVT quantiles plotted against itself which serves as the reference line. c) Semi-log probability distribution of multimodel mean IVT at 34S in the historical 1980-2014 (purple), SSP245 2080-2100 (yellow) and SSP585 2080-2100 (orange) model runs, and ERA5 IVT distribution 1980-2014

(blue dashed line). d) Consecutive days exceeding the 85th percentile IVT in the historical run of each model for the historical (purple), SSP245 (yellow) and SSP585 (orange) scenarios.

Bar values are the multimodel mean while error bars represent the model spread. All multimodel means only include the top 8 models.

We evaluated the model simulations of IVT over Sydney by comparing the probability distributions of each model to the probability distribution of IVT in ERA5. Figures 3a-b show the quantile-quantile plot of ERA5 IVT versus each model. The black line is the ERA5 distribution plotted against itself which serves as a reference line. The closer the models are to this reference line the better they simulate the observed distribution of IVT over Sydney. The eight best-performing models are displayed in Figure 3b. The model spread and displacement from the black reference line is considerably smaller in Figure 3b compared to Figure 3a. The multimodel mean values calculated in subsequent figures only incorporate the best eight models.

The models typically have a negative IVT bias at lower values. However, the models perform well above the commonly used IVT threshold for defining ARs ($250\text{Kg m}^{-1} \text{s}^{-1}$ [Shields et al. 2018]), which is when we expect to observe more impactful rain events. The worst performing model deviates from the ERA5 99th percentile IVT by $130\text{Kg m}^{-1} \text{s}^{-1}$ (BCC-CSM2-MR), while the best performing model deviates by only $15.5\text{Kg m}^{-1} \text{s}^{-1}$ (EC-Earth3). We note that we did also examine the projections in all models, including the models that performed poorly in our historical evaluation, and found the sign of future IVT change was consistent across all models though the magnitude varied considerably. The range of IVT magnitude projections narrowed when we excluded the weaker models. We include versions of Figures 3C and 4 that incorporate all models in the Supplementary Material.

After evaluating the models, we could then analyze their IVT projections with some confidence. Figure 3c shows the multimodel mean normalized probability distribution of IVT for the historical period (1980-2014) and future (2080-2100) under SSP245 and SSP585. The probability distribution is shown as a semi-log plot so that the relative difference in frequency at the extreme end of the distribution is clearer. The distribution in ERA5 is also shown in blue. We see a positive shift in both future distributions with respect to the historical period. Above about $300 \text{ Kg m}^{-1} \text{ s}^{-1}$, the difference in frequency between the historical and future IVT values exceeds the difference between the frequency in the historical and ERA5 distributions. This indicates that there is a robust projected increase in extreme IVT by the end of the century under both SSPs, however the magnitude of change in the median IVT is much more uncertain. The question of when a climate change signal in IVT emerges over this region is a potential avenue for future research as we found a minimal shift in the IVT probability distribution between 2030-2050, but a stronger signal between 2080-2100 (Supplementary Figure 3).

The duration of high IVT over a region is an important factor that determines the severity of extreme hydrological events and was particularly notable during the March 2021 floods. Therefore, we examined the projected future changes to the duration of high IVT events in Figure 3d. High IVT events were defined using a relative threshold to account for differences in the water vapor content of the models as recommended by Rutz et al., (2019). We used the 85th percentile of IVT in the historical run of each model because this value is often used to define the boundary of ARs (Shields et al., 2018) and is approximately $250 \text{ Kg m}^{-1} \text{ s}^{-1}$ in ERA5. We then calculated the consecutive number of days exceeding this threshold in the historical and future projections. Our results indicate that the frequency of multiday high IVT

events is likely to increase under SSP245 and SSP585. We see a robust increase in the frequency of 2-day high IVT events of about 40%, as indicated by the model range (error bars) of the historical period not overlapping with the range in the future scenarios, and a less robust increase in 3-day and 4-day events. Although, we cannot confidently draw conclusions about the highest impact 5-day and longer events likely due to a very limited sample size.

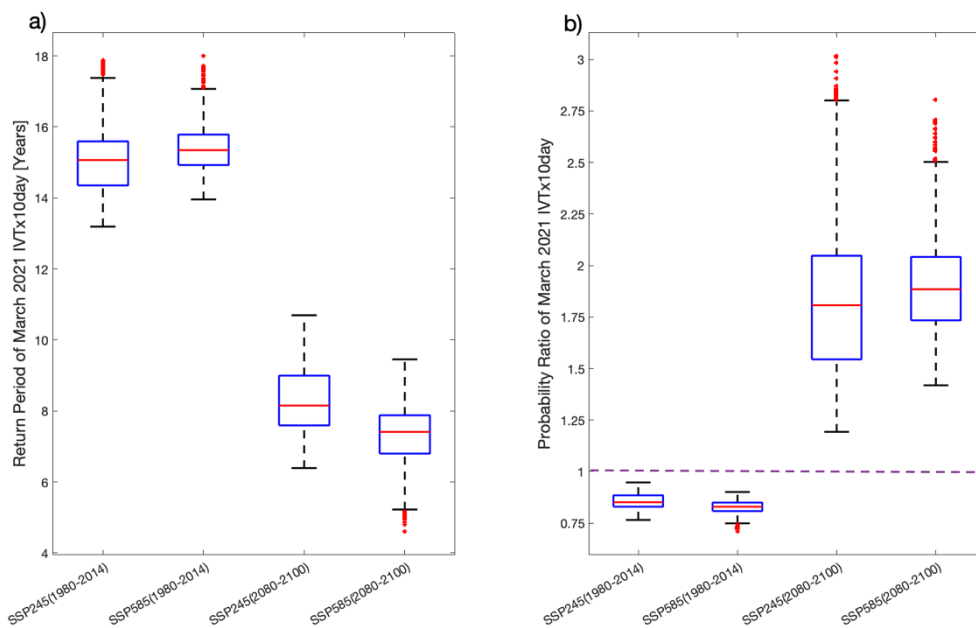


Figure 4: a) Range of return period and b) probability ratio of an IVTx10day event of equivalent magnitude to the March 2021 event under historical (1980-2014) and future (2080-2100) SSP245 and SSP585 conditions.

Given the high uncertainty in the most extreme IVT events due to the small sample size, we undertook a GEV modelling analysis to further understand how the likelihood of extreme IVT events may change in a warmer climate. The return period of IVTx10day equivalent to the March 2021 event almost halves between the historical and future periods under both SSPs. We observe a strong reduction in the return periods (Figure 4a) indicating that events akin to that of March 2021 would become more regular under the projected scenarios. While the end-of-century return periods are significantly lower than the historical return periods, the

differences between return periods projected by the two scenarios are statistically indistinguishable. The probability ratio of IVT_{x10day} has a large uncertainty range under both scenarios but is consistently greater than one indicating that all CMIP6 models indicate an increase in probability of events as rare as the observed March 2021 event.

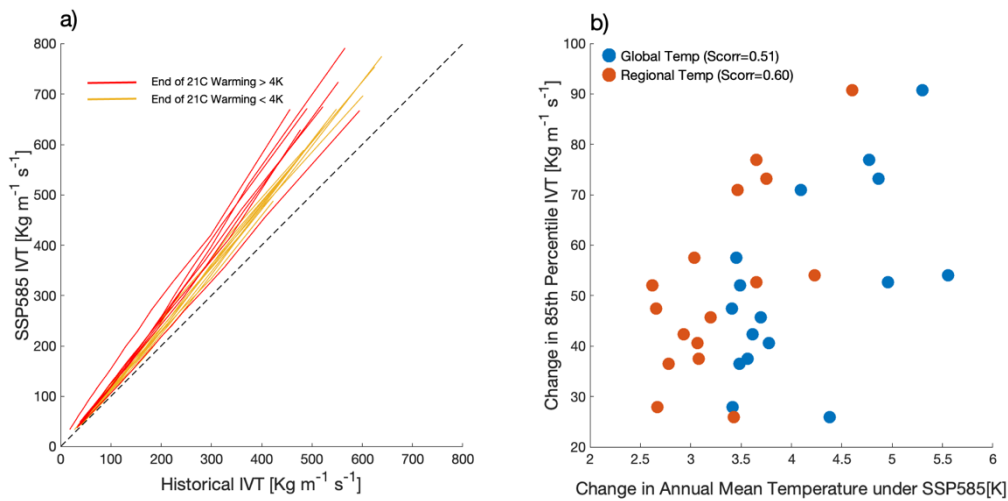


Figure 5: a) Quantile-quantile plot of historical (1980-2014) versus SSP585 (2080-2100) IVT for each of the 16 models. Yellow lines indicate models where the difference in global mean temperature between the pre-industrial period (1850-1880) and end of 21st Century (2080-2100) was below 4K, while red lines are models where the change in global mean temperature exceeded 4K. The black dashed line is the one-to-one reference. b) Scatter plot of the change in global (blue) and regional (orange; 80-180E, 50-0S) mean temperature under SSP585 in each model versus the change in the 85th percentile of IVT between the historical and future periods. Scorr is the Spearman Rank Correlation Coefficient and both of these were statistically significant ($p < 0.05$).

Given the range in climate sensitivity within the CMIP6 ensemble (Meehl et al., 2020; Zelinka et al., 2019) we hypothesized that differences in climate sensitivity may affect out

results. To test this, we calculated the change in global mean temperature between the pre-industrial period (1850-1880) and end of 21st Century (2080-2100). We found that the models with a faster rate of warming all projected higher IVT increases (Figure 5a) except for one model which we discuss in the following paragraphs. This is an important result as it indicates that uncertainty of climate sensitivity may increase the spread of projections of moisture flux and therefore affect projected changes in precipitation extremes.

Moreover, we found a strong relationship between the global and regional mean temperature change and the value of the 85th percentile of IVT which is commonly used to define Atmospheric Rivers (Figure 5b). Regional here refers to between 80°E-180°E longitude and 50°S-0°S latitude. IVT appears to be slightly more correlated to regional temperatures than global temperatures, suggesting that studies of moisture flux and climate change should consider the rate of global and regional warming in the models.

Model representation of the jet stream and associated storm tracks likely affects IVT projections. Simpson et al., (2020) evaluated CMIP6 representation of midlatitude phenomena and found that the majority of CMIP6 models positioned the Southern Hemisphere (SH) jet too far equatorward. We note that the ensemble member that overestimated IVT the most in the historical model run (BCC-CSM2-MR) also considerably overestimates the speed of the SH jet (Simpson et al., 2020). Furthermore, despite a relatively fast rate of warming in AWI-CM-1-1-MR, that model projects the smallest IVT increase over Sydney by the end of the 21st Century, whereas across the other models there is a strong relationship between rate of warming and IVT increase. However, according to Simpson et al. (2020), AWI-CM-1-1-MR is one of the best models at simulating both the position and speed of the SH jet. Global circulation changes such as the position and speed of the jet and

frequency of blocking are likely sources of uncertainty in future precipitation changes (Nishant & Sherwood, 2021)

Conclusion

IVT is a useful tool for understanding how hydrological extremes may change in the future.

IVT is often better represented in models than precipitation and is highly correlated to precipitation. Extreme multi-day rainfall and flooding in Sydney occurred in March 2021 during a period of persistent and intense water vapor transport over the region. We have examined the IVT for this event, placed it in the context of the observational record, and evaluated how the distribution of IVT changes in a warmer climate using CMIP6 models.

The maximum daily IVT during the event was the top 0.3% of daily IVT since 1980 and the 3rd highest 10-day IVT mean. We found that both the intensity of IVT and the frequency of persistent IVT events will likely increase under SSP245 and SSP585, with SSP585 leading to stronger increases. The probability of events of a similar magnitude to the March 2021 event will increase by approximately 80% with the interquartile range of estimates varying from 50-100% (Figure 4) by the end of the 21st Century over Sydney under both moderate and high emissions scenarios. Lastly, we found that the change in IVT is proportional to the rate of warming. Models with faster warming tend to project larger increases in IVT. We have not considered, and there has been limited research to date on, the weather systems that produce these extreme IVT events and their representation in climate models over this region. The analysis herein has demonstrated that the IVT associated with this event was extreme, but not unprecedented. However, the balance of evidence from the considered climate projections suggests that intense and persistent IVT events like this will occur more often in the future.

Acknowledgements:

This article is protected by copyright. All rights reserved.

The work of K J Reid was funded by an Australian Government Research Training Program (RTP) Scholarship and the Australian Research Council (ARC; DE180100638), the work of A D King was funded by the ARC (DE180100638), and the work of T P Lane was funded by the ARC Centre of Excellence for Climate Extremes (CE170100023).

We acknowledge the World Climate Research Programme, which, through its Working Group on Coupled Modelling, coordinated and promoted CMIP6. We thank the climate modelling groups for producing and making available their model output, the Earth System Grid Federation (ESGF) for archiving the data and providing access, and the multiple funding agencies who support CMIP6 and ESGF.

The work of T.A. O'Brien was supported in part by the U.S. Department of Energy, Office of Science, Office of Biological and Environmental Research, Climate and Environmental Sciences Division, Regional & Global Model Analysis Program, under Award Number DE-AC02-05CH11231; in part by the Environmental Resilience Institute, funded by Indiana University's Prepared for Environmental Change Grand Challenge initiative and in part by Lilly Endowment, Inc., through its support for the Indiana University Pervasive Technology Institute.

This research was undertaken with the assistance of resources from the National Computational Infrastructure (NCI Australia) supported by the Australian Government. Additionally, we thank Scott Wales for helping write the script used to obtain the CMIP6 data.

K.J. Reid ORCID: 0000-0001-5972-6015

T.A. O'Brien ORCID: 0000-0002-6643-1175

A.D. King ORCID: 0000-0001-9006-5745

T.P. Lane ORCID: 0000-0003-0171-6927

Data Availability:

The ERA5 (10.24381/cds.adbb2d47) and CMIP6 (<https://esgf-node.llnl.gov/projects/cmip6/>) datasets used in this study are publicly available.

References:

- The Bureau of Meteorology. (2021). *Special Climate Statement 74-extreme rainfall and flooding in eastern and central Australia in March 2021*.
- The Bureau of Meteorology. (2012). *Monthly Weather Review New South Wales*. Retrieved from <http://www.ag.gov.au/cca>.
- Corringham, T. W., Martin Ralph, F., Gershunov, A., Cayan, D. R., & Talbot, C. A. (2019). Atmospheric rivers drive flood damages in the western United States. *Science Advances*, 5(12), eaax4631. <https://doi.org/10.1126/sciadv.aax4631>
- Eyring, V., Bony, S., Meehl, G. A., Senior, C. A., Stevens, B., Stouffer, R. J., & Taylor, K. E. (2016). Overview of the Coupled Model Intercomparison Project Phase 6 (CMIP6) experimental design and organization. *Geoscientific Model Development*, 9(5), 1937–1958. <https://doi.org/10.5194/GMD-9-1937-2016>
- Foreman-Mackey, D., Farr, W. M., Sinha, M., Archibald, A. M., Hogg, D. W., Sanders, J. S., et al. (2019). emcee v3: A Python ensemble sampling toolkit for affine-invariant MCMC. *Journal of Open Source Software*, 4(43), 1864. <https://doi.org/10.21105/joss.01864>
- Gimeno, L., Dominguez, F., Nieto, R., Trigo, R., Drumond, A., Reason, C. J. C., et al. (2016). Major Mechanisms of Atmospheric Moisture Transport and Their Role in Extreme Precipitation Events. *Annual Review of Environment and Resources*, 41(1), 117–141. <https://doi.org/10.1146/annurev-environ-110615-085558>
- Hersbach, H., Bell, B., Berrisford, P., Horányi, A., Sabater, J. M., Nicolas, J., et al. (2019).

Global reanalysis: goodbye ERA-Interim, hello ERA5. *ECMWF Newsletter*, (159), 17–24. <https://doi.org/10.21957/vf291hehd7>

Lavers, D. A., & Villarini, G. (2013). The nexus between atmospheric rivers and extreme precipitation across Europe. *Geophysical Research Letters*, 40(12), 3259–3264. <https://doi.org/10.1002/grl.50636>

Lavers, D. A., & Villarini, G. (2015). The relationship between daily European precipitation and measures of atmospheric water vapour transport. *International Journal of Climatology*, 35(8), 2187–2192. <https://doi.org/10.1002/joc.4119>

Lavers, D. A., Pappenberger, F., & Zsoter, E. (2014). Extending medium-range predictability of extreme hydrological events in Europe. *Nature Communications*, 5(1), 1–7. <https://doi.org/10.1038/ncomms6382>

Ma, W., Chen, G., & Guan, B. (2020). Poleward Shift of Atmospheric Rivers in the Southern Hemisphere in Recent Decades. *Geophysical Research Letters*, 47(21), e2020GL089934. <https://doi.org/10.1029/2020GL089934>

Meehl, G. A., Senior, C. A., Eyring, V., Flato, G., Lamarque, J. F., Stouffer, R. J., et al. (2020, June 1). Context for interpreting equilibrium climate sensitivity and transient climate response from the CMIP6 Earth system models. *Science Advances*. American Association for the Advancement of Science. <https://doi.org/10.1126/sciadv.aba1981>

Nicholls, N. (2006). *Introduction: what is climate change detection and attribution? Detecting and attributing Australian climate change: a review*. *Aust. Met. Mag* (Vol. 55).

Nishant, N., & Sherwood, S. C. (2021). How Strongly Are Mean and Extreme Precipitation Coupled? *Geophysical Research Letters*, 48(10), e2020GL092075. <https://doi.org/10.1029/2020gl092075>

O'Neill, B. C., Tebaldi, C., Van Vuuren, D. P., Eyring, V., Friedlingstein, P., Hurtt, G., et al.

(2016). The Scenario Model Intercomparison Project (ScenarioMIP) for CMIP6. *Geoscientific Model Development*, 9(9), 3461–3482. <https://doi.org/10.5194/gmd-9-3461-2016>

Perkins, S. E., Pitman, A. J., Holbrook, N. J., & McAneney, J. (2007). Evaluation of the AR4 climate models' simulated daily maximum temperature, minimum temperature, and precipitation over Australia using probability density functions. *Journal of Climate*, 20(17), 4356–4376. <https://doi.org/10.1175/JCLI4253.1>

Reid, K. J., Rosier, S. M., Harrington, L. J., King, A. D., & Lane, T. P. (2021). Extreme rainfall in New Zealand and its association with Atmospheric Rivers. *Environmental Research Letters*, 16(4), 044012. <https://doi.org/10.1088/1748-9326/abeae0>

Risser, M. D., & Wehner, M. F. (2017). Attributable Human-Induced Changes in the Likelihood and Magnitude of the Observed Extreme Precipitation during Hurricane Harvey. *Geophysical Research Letters*, 44(24), 12,457–12,464. <https://doi.org/10.1002/2017GL075888>

Rutz, J. J., Steenburgh, W. J., & Ralph, F. M. (2014). Climatological Characteristics of Atmospheric Rivers and Their Inland Penetration over the Western United States. *Monthly Weather Review*, 142(2), 905–921. <https://doi.org/10.1175/MWR-D-13-00168.1>

Rutz, J. J., Shields, C. A., Lora, J. M., Payne, A. E., Guan, B., Ullrich, P., et al. (2019). The Atmospheric River Tracking Method Intercomparison Project (ARTMIP): Quantifying Uncertainties in Atmospheric River Climatology. *Journal of Geophysical Research: Atmospheres*, 124(24), 13777–13802. <https://doi.org/10.1029/2019JD030936>

Shields, C. A., Rutz, J. J., Leung, L.-Y., Ralph, F. M., Wehner, M., Kawzenuk, B., et al. (2018). Atmospheric River Tracking Method Intercomparison Project (ARTMIP): project goals and experimental design. *Geosci. Model Dev*, 11, 2455–2474.

<https://doi.org/10.5194/gmd-11-2455-2018>

- Simpson, I. R., Bacmeister, J., Neale, R. B., Hannay, C., Gettelman, A., Garcia, R. R., et al. (2020). An Evaluation of the Large-Scale Atmospheric Circulation and Its Variability in CESM2 and Other CMIP Models. *Journal of Geophysical Research Atmospheres*, 125. <https://doi.org/10.1029/2020JD032835>
- Stephens, G. L., L'Ecuyer, T., Forbes, R., Gettelmen, A., Golaz, J.-C., Bodas-Salcedo, A., et al. (2010). Dreary state of precipitation in global models. *Journal of Geophysical Research: Atmospheres*, 115(D24). <https://doi.org/10.1029/2010JD014532>
- Swart, N. C., Fyfe, J. C., Gillett, N., & Marshall, G. J. (2015). Comparing trends in the southern annular mode and surface westerly jet. *Journal of Climate*, 28(22), 8840–8859. <https://doi.org/10.1175/JCLI-D-15-0334.1>
- The Bureau of Meteorology. (2012). *Monthly Weather Review New South Wales*. Retrieved from <http://www.ag.gov.au/cca>.
- The Bureau of Meteorology. (2021). *Special Climate Statement 74-extreme rainfall and flooding in eastern and central Australia in March 2021*.
- Viale, M., Valenzuela, R., Garreaud, R. D., & Ralph, F. M. (2018). Impacts of Atmospheric Rivers on Precipitation in Southern South America. *Journal of Hydrometeorology*, 19(10), 1671–1687. <https://doi.org/10.1175/JHM-D-18-0006.1>
- Warner, M. D., Mass, C. F., & Salathé, E. P. (2015). Changes in Winter Atmospheric Rivers along the North American West Coast in CMIP5 Climate Models. *Journal of Hydrometeorology*, 16(1), 118–128. <https://doi.org/10.1175/JHM-D-14-0080.1>
- Zelinka, M. D., Myers, T. A., Mccoy, D. T., Po-Chedley, S., Caldwell, P. M., Ceppi, P., et al. (2019). Causes of Higher Climate Sensitivity in CMIP6 Models. *Geophysical Research Letters*. <https://doi.org/10.1029/2019GL085782>